Available online at www.sciencedirect.com

SCIENCE DIRECT®

Earth and Planetary Science Letters 233 (2005) 337–349

EPSL

www.elsevier.com/locate/epsl

Thermal structure of oceanic and continental lithosphere

Dan McKenzie*, James Jackson, Keith Priestley

Institute of Theoretical Geophysics, Bullard Labs, Madingley Road, Cambridge CB3 0EZ, U.K.

Received 3 September 2004; received in revised form 1 February 2005; accepted 10 February 2005
Available online 8 April 2005
Editor: V. Courtillot

Abstract

Recent studies of the focal depths of earthquakes in old continental lithosphere have shown that they are almost entirely confined to the crust. Except where recent subduction of oceanic lithosphere is likely to have occurred, no earthquakes with a magnitude of >5.5 have yet been located beneath the Moho. In contrast, in oceanic lithosphere earthquakes commonly occur within the mantle. The principal control on whether or not deformation occurs by brittle failure has long been believed to be temperature. We re-examine the thermal models of both oceans and shields. Taking account of the temperature dependence of the thermal conductivity lowers the temperature within the oceanic lithosphere. Except beneath the outer rises of trenches, where the strain rates are large, intraplate oceanic earthquakes are confined to regions cooler than 600 °C. In continental regions most earthquakes occur in the mobile belts that surround Archaean cratons, where the crust is as thick as 50–60 km. Recent studies, of the Canadian Shield in particular, have shown that radiogenic heating is not as concentrated at shallow depths as was previously believed. Taking account of both these effects and the temperature dependence of the thermal conductivity increases the Moho temperatures, which can exceed 600 °C, and produces geotherms that agree well with pressure and temperature estimates from nodule suites from kimberlites. Therefore the mechanical behaviour of oceanic and continental upper mantle appears to depend on temperature alone, and there is as yet no convincing evidence for any compositional effects.

Keywords: heat flow; oceanic bathymetry; mantle rheology; continental geotherms

1. Introduction

The mechanical properties of the lithosphere allow elastic stresses to be transmitted over large distances, and therefore permit plates as large as the Pacific Plate to move as rigid caps bounded by faults that generate earthquakes. The thickness of the elastic part of the lithosphere also controls the extent of isostatic compensation, which can be estimated from the transfer function between gravity and topography. In oceanic lithosphere the thickness T_s, of the seismogenic layer is slightly larger than the elastic thickness T_e, estimated from gravity and topography (see [1]), perhaps because the time scale for the accumulation and release of seismic stresses is much shorter than

* Corresponding author. Tel.: +44 1223 337177.
E-mail address: mckenzie@esc.cam.ac.uk (D. McKenzie).

0012-821X/$ - see front matter © 2005 Elsevier B.V. All rights reserved.
doi:10.1016/j.epsl.2005.02.005

that for the accumulation and removal of topographic loads. Furthermore the values of both T_s and T_e increase monotonically with the age of the plate. The temperature structure within oceanic plates is generally calculated from the plate model, which assumes that the lithosphere is created at a constant temperature and cools with age, and that the base temperature is constant everywhere. It is surprising that this simple model provides an accurate description of the variation of depth and heat flow with age. Oceanic plates form the upper boundary layer of the convective circulation which extends throughout the mantle and which must involve considerable temperature variations. However, there is little evidence of such variations in the upper mantle beneath the plates, except where it is influenced by plumes. The thickness of the oceanic crust and the S wave velocity below the plates are both sensitive to small variations in mantle potential temperature. Increasing the potential temperature by 12.5 °C increases the crustal thickness by 1 km. Where the crustal thickness is not affected by plumes or fracture zones its value is 7.1 ± 0.8 km [2]. This standard deviation corresponds to a temperature variation of only 10 °C. Shear wave velocity variations beneath oceanic plates can also be used to constrain temperature variations (Priestley and McKenzie in prep.), and give values of no more than a few tens of degrees. The unexpectedly small magnitude of these temperature variations is presumably the reason why the plate model is so successful. The temperature within the cooling plate can be calculated analytically. The resulting depth of the 700 °C isotherm is equal or greater than the value of T_e [1], and that of the 800 °C isotherm is equal or greater than the value of T_s [3,4].

There is less agreement about the behaviour of continental lithosphere. Careful studies of earthquake depths have now shown that almost all events occur within the continental crust [5–7] (Fig. 1). The deepest events with depths of 85–90 km occur very close to the Moho beneath the Himalaya [6,7], where the Indian Shield is being overthrust by Tibet and the temperature is controlled by downward advection and so is difficult to estimate. Such calculations are easier to carry out for Archaean and Proterozoic shields, where the temperature has reached steady state and where the crustal thickness is in places as great as 55–60 km. Most estimates of T_e, for continental regions have been obtained using Forsyth's [8] coherence method, and those for a number of shields exceed 100 km. However it is difficult to understand how T_e can exceed T_s. Recently McKenzie and Fairhead [9] and McKenzie [10] have argued that the value of T_e obtained by Forsyth's method should always exceed

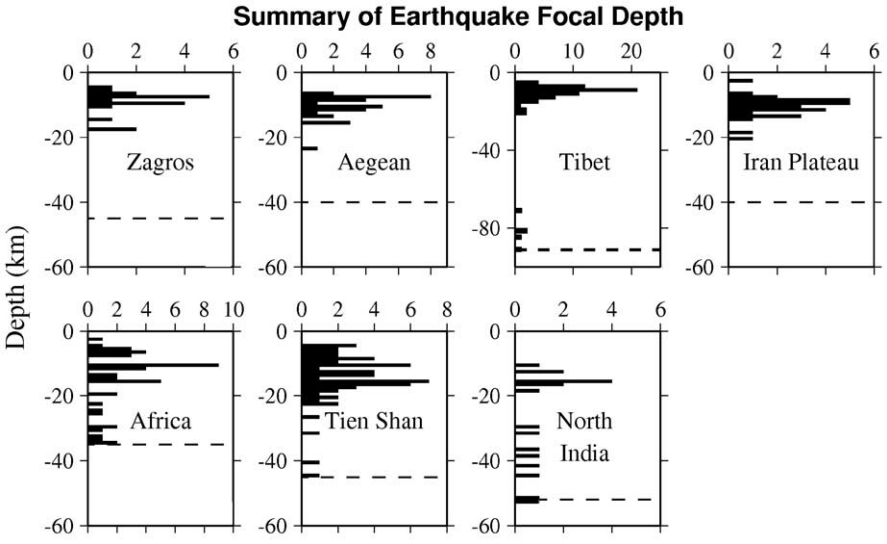

Fig. 1. The depths of earthquakes, obtained by waveform modelling [11], in various continental regions where lower crustal earthquakes occur. The dashed lines show the depth of the Moho estimated using receiver functions [5,6,11]. Notice that the depth scale for Tibet is different from that of the other regions.

the true value of T_e which therefore provides an upper bound, rather than estimate, of its value. They instead used the transfer function between topography and free air gravity to estimate T_e, and obtained values that are everywhere less than T_s, [11], in agreement with the rheological behaviour of continental and oceanic lithosphere. Artemieva and Mooney [12] estimated the temperature at the Moho beneath Archaean shields to be 300–500 °C. If the continental upper mantle behaves in the same way as the oceanic lithosphere, it should therefore be able to support stresses for geological times and to generate earthquakes. Yet it does neither (Fig. 1). Maggi et al. [11] suggested that the difference in behaviour might be caused by the presence of hydrous minerals, which weaken olivine and pyroxene.

However, a simpler alternative explanation which we examine here is that the accepted estimates of the temperatures within both the continental and oceanic lithosphere are less accurate than is commonly believed. The temperature structure of the oceanic lithosphere is generally estimated from the variation of depth and heat flow with age [13–15] using a simple analytic model for a cooling plate that assumes the thermal expansion coefficient, the thermal conductivity, and the initial temperature are all constant. Though these assumptions are known to be incorrect, it has usually been assumed that the simple analytic expressions are sufficiently accurate for geophysical discussions. Doin and Fleitout [16] obtained numerical solutions when the specific heat and thermal conductivity depended on temperature, and the thermal expansion coefficient on both temperature and pressure. They used a fixed heat flux boundary condition at the base of the plate. Since the heat flux within the old plate must be independent of depth, the constant heat flux in their model must be the same as the surface heat flux through old sea floor. This boundary condition requires temperature gradients to exist at the base plate beneath ridge axes. In such regions the temperature is generally believed to be controlled by isentropic upwelling. The resulting temperature gradient is about a factor of twenty smaller than that beneath old sea floor. There is therefore no obvious physical process that can maintain a constant heat flux at the base of the plate. For this reason we use constant temperature, rather than heat flux, as the boundary condition.

For continental lithosphere the model that is still most often used to calculate the temperature is that of Pollack and Chapman [17]. They assumed that the temperature had reached steady state, and that the crustal radiogenic heat production was strongly concentrated towards the surface. They did not require their geotherms to converge on a single mantle geotherm below the lithosphere. Jaupart, Mareschal and their co-workers [18–20] have made a detailed study of the surface heat flow and radioactivity of the surface of the Canadian Shield, and argue that the radiogenic heat production in granulite facies terrains does not decrease strongly with depth, and that the heat flux through the Moho is only about half of that estimated by Pollack and Chapman [17]. In contrast to the oceanic lithosphere, where no direct estimates of the temperature can be obtained, the mineral compositions from garnet peridotite nodules can be used to estimate both the depths and temperatures at which such nodules equilibrated. A considerable number of such nodule suites have now been studied, and the resulting estimates of temperature and depth can be used to construct steady state geotherms for various continental regions. The accuracy of such geotherms from the Canadian Shield can be tested using the heat flow. The geotherms can also be used to estimate the temperature at the Moho, to test whether the simplest rheological model, where the mechanical properties of the mantle part of the lithosphere are controlled by temperature alone, is sufficient to account for the distribution of earthquake depths.

2. Modelling the temperature structure

2.1. Oceans

The thermal model which has been extensively used to estimate the temperature structure of oceanic lithosphere was originally proposed by McKenzie [21]. It consists of a plate of thickness a that is generated at a constant temperature T_1 beneath a ridge spreading with constant velocity V (Fig. 2). If the thermal conductivity k is constant, it is straightforward to obtain an analytic expression for the temperature within the plate, and to show the geotherm depends only on the age of the plate when V exceeds about 10 mm a^{-1}. It is also straightforward to

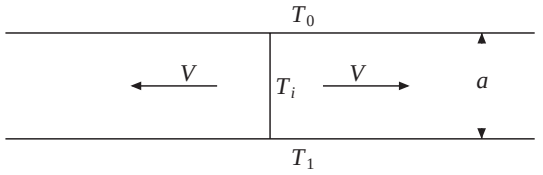

Fig. 2. Model used to calculate the variation of depth and heat flux with the age of an oceanic plate.

calculate the variation of depth with age if the plate is isostatically compensated and the thermal expansion coefficient α is constant. Parsons and Sclater [13] used observed values of depth in various oceans to estimate the best fitting values of a, T_1, k and α. The values they obtained for the North Pacific were $a=125$ km, $T_1=1333$ °C, $k=3.14$ W m^{-1} K^{-1} and $\alpha=3.28\times10^{-5}$ K^{-1}. Sclater et al. [14] showed that the resulting model was also consistent with the reliable heat flow observations. The same approach was used by Stein and Stein [15], who argued that $a=95$ km, $T_1=1450$ °C, $k=3.138$ W m^{-1} K^{-1} and $\alpha=3.1\times10^{-5}$ K^{-1} fitted the data better than the values estimated by Parsons and Sclater [13].

An alternative approach is to calculate the thermal structure using values of k and α for peridotite measured in the laboratory. Furthermore, if decompression melting is to produce an oceanic crustal thickness of 7 km, the temperature at which the plate is formed can no longer be freely adjusted. This constraint fixes the potential temperature of the mantle and the variation of temperature with depth beneath the ridge axis, which is taken to be the initial temperature T_i of the plate. Only the thickness a of the plate then remains as an adjustable parameter to fit the depth and heat flow observations. The agreement between the calculations and the observations is therefore a more severe test of the model in Fig. 2 than are the tests carried out by Parsons and Sclater and by Stein and Stein. Moreover, if the tests are satisfactory, the calculated temperature structure is also likely to be more accurate.

The experimental values of the thermal conductivity k for forsterite, measured by Schatz and Simmons [22], are plotted in Fig. 3 and vary by about a factor of two in the temperature range of interest, 370–1500 K. Because the concentrations of K,U and Th are so low in the upper mantle, and because these elements are removed from the mantle by melt generation, radioactive heat generation within the oceanic lithosphere is ignored. If horizontal heat conduction is also ignored, the temperature $T=T(z,t)$ within a cooling plate satisfies

$$\frac{\partial[\rho(T)C_P(T)T]}{\partial t}=\frac{\partial}{\partial z}\left(k(T)\frac{\partial T}{\partial z}\right) \quad (1)$$

in a reference frame moving with the plate. The origin is taken to be at the Earth's surface, and z to increase downwards. This equation is clearly nonlinear in T, which complicates the problem of obtaining a numerical solution. If an analytic expression for the integral

$$G=\int k(T)\mathrm{d}T \quad (2)$$

can be obtained, Eq. (1) can be written

$$\frac{\partial T}{\partial t}=\frac{1}{\rho C_P}\frac{\partial^2 G}{\partial z^2}-\frac{T}{\rho C_P}\frac{\partial(\rho C_P)}{\partial t}. \quad (3)$$

The second term on the right is considerably smaller than the first. If it is ignored, the resulting equation can be solved by standard methods. The solution to the full equation can then be obtained by iteration. Inclusion of the second term changes the temperature by less than 5 °C.

Hofmeister [24] reviewed experimental and theoretical estimates of $k=k(T)$, and proposed analytical expressions for the temperature dependence. Thermal conductivity is controlled by two processes. The first

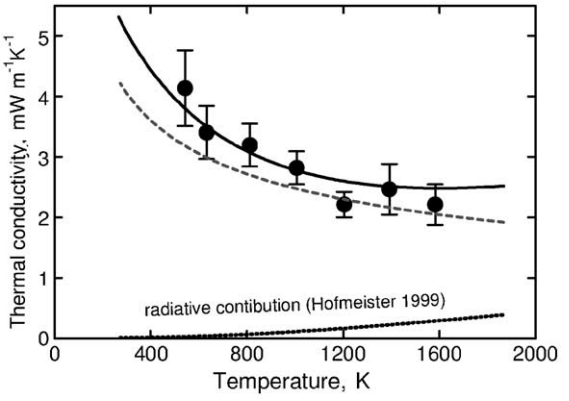

Fig. 3. The variation of the thermal conductivity with temperature. The data points and their uncertainties are taken from Schatz and Simmons [22]. The solid line is calculated from Eq. (4) and the dashed line from the expression of Xu et al's [23], Eq.(6).

is heat transport by phonons. As the temperature increases, so does the phonon density, but the mean free path between their collisions decreases. The second process is radiative transfer of heat by photons. The efficiency of this process increases with temperature, but its importance is strongly affected by the presence of iron in olivine and pyroxene. Hofmeister [24] gives a simple polynomial expression for the radiative contribution to $k(T)$ whose integration is trivial. However, her expression for the phonon contribution is not easily integrated. Therefore a simpler expression was used

$$k_{\mathrm{H}}(T) = \frac{b}{1+cT} + \sum_{m=0}^{3} d_m (T+273)^m \tag{4}$$

which differs from hers by less than the standard deviation of the experiments in the temperature interval of interest (Fig. 3). Hence

$$G_{\mathrm{H}} = \frac{b}{c}\log_e(1+cT) + \sum_{m=0}^{3} \frac{d_m}{m+1}(T+273)^{m+1} \tag{5}$$

where T is the temperature in degrees centigrade. The values used for the constants are $b=5.3$, $c=0.0015$, $d_0=1.753\times10^{-2}$, $d_1=-1.0365\times10^{-4}$, $d_2=2.2451\times10^{-7}$, $d_3=-3.4071\times10^{-11}$ $k(T)$, calculated from Eq. (5), is plotted in Fig. 3, and shows that the radiative contribution to $k_{\mathrm{H}}(T)$ is small. Because the uncertainties in $k(T)$ are still quite large, we also used an alternative expression for $k(T)$ for olivine that has recently been proposed by Xu et al. [23] (Fig. 3)

$$k_{\mathrm{X}}(T) = k_{298}(298/(T+273))^n \tag{6}$$

where $k_{298}=4.08$ W m^{-1} K^{-1}, $n=0.406$. The corresponding expression for G is

$$G_{\mathrm{X}} = k_{298}298^n(T+273)^{1-n}/(1-n). \tag{7}$$

Numerical calculations were carried out using both G_{H} (Eq.(5)) and G_{X} (Eq.(7)), to explore the effect of using different expressions for $k=k(T)$ on the calculated temperature structure.

The standard analytical model ignores the variation of ρ and C_{P} with temperature. Though the effect of such variations are small, they are easily included in a numerical scheme, and should be taken into account for self-consistency. Furthermore the variation of depth with age is controlled by the temperature dependence of ρ. Bouhifd et al. [25] made careful measurements of $\alpha(T)$ from 599 to 2100 K and found an increase of almost a factor of two. They show that their results agree with those of several other groups Bouhifd et al. parameterise their observations using

$$\alpha(T) \equiv -\frac{1}{\rho}\left(\frac{\partial\rho}{\partial T}\right)_{\mathrm{P}} = \alpha_0 + \alpha_1 T \tag{8}$$

where $\alpha_0=2.832\times10^{-5}$ and $\alpha_1=3.79\times10^{-8}$ are constants. Integration gives

$$\rho(T) = \rho_0 \exp\left(-\left[\alpha_0(T-T_0) + \frac{\alpha_1}{2}\left(T^2-T_0^2\right)\right]\right) \tag{9}$$

where $T_0=273$ K and $\rho_0=3.33$ Mg m^{-3}.

The variation of specific heat with temperature $C_{\mathrm{P}}(T)$makes an important contribution to thermodynamic stability calculations, and has therefore been accurately determined. We used Berman and Aranovich's [26] expression for $C_{\mathrm{P}}(T)$ in kJ/mol

$$C_{\mathrm{P}}(T) = k_0 + k_1 T^{-1/2} + k_3 T^{-3} \tag{10}$$

where $k_0=233.18$, $k_1=-1801.6$ and $k_3=-26.794\times10^7$ for forsterite, and $k_0=252$, $k_1=-2013.7$ and $k_3=-6.219\times10^7$ or fayalite. We assumed that the molar fraction of fayalite in the mantle is 0.11.

We used the numerical scheme from Press et al. ([27], p 842) to solve Eq. (3), which is properly centred in time and space, and initially ignored the second term on the right hand side

$$\begin{aligned} &-Ak_{j-1}^n T_{j-1}^{n+1} + \left(1+2Ak_j^n\right)T_j^{n+1} - Ak_{j+1}^n T_{j+1}^{n+1} \\ &\quad = T_j^n + 2A\left(G_{j+1}^n - 2G_j^n + G_{j-1}^n\right) \\ &\qquad - A\left(k_{j+1}^n T_{j+1}^n - 2k_j^n T_j^n + k_{j-1}^n T_{j-1}^n\right) \end{aligned} \tag{11}$$

where

$$A = \frac{\Delta t}{2\rho\left(T_j^n\right)C_{\mathrm{P}}\left(T_j^n\right)\Delta z^2}$$

and Δt is the time step, Δz the mesh size, and G_j^n is the value of the variable G at $z=j\Delta z$, $t=n\Delta t$. Eq. (11) was solved by tridiagonal elimination using 100 mesh intervals, with $\Delta t=\Delta z^2/(2.2\kappa_{\mathrm{m}})$, where κ_{m}, is the maximum value of $\kappa=k(T)/\rho(T)C_{\mathrm{P}}(T)$, in the plate.

Once a solution for T_j^{n+1} had been obtained, a correction term

$$-\frac{\left(T_j^{n+1}+T_j^n\right)\left[(\rho C_P)_j^{n+1}-(\rho C_P)_j^n\right]}{\left[(\rho C_P)_j^{n+1}+(\rho C_P)_j^n\right]}$$

was added to the right hand side of Eq. (11) and the solution for T_j^{n+1} recalculated. This procedure was repeated until the maximum temperature difference between iterations became less than 0.1 °C. At ages of less than 2 Ma four iterations were required, falling to two when the age exceeded about 30 Ma. The accuracy of the numerical scheme was tested by comparison with the analytical solution, by using $G=kT$, where k is the constant value of the thermal conductivity, and constant values of ρ and C_P. The root mean square error (rms) was less than 1.5 °C.

An advantage of solving Eq. (1) numerically is that it is easy to impose an arbitrary initial temperature beneath the ridge axis. That used here was obtained by choosing the potential temperature T_P of the mantle beneath the plate so that a crustal thickness of 7 km was generated by decompression melting. This approach gave a value of 1315 °C for T_P when the entropy of melting ΔS was 400 J K^{-1} kg^{-1} [28]. The uncertainty in ΔS is about 10% [28], corresponding to an uncertainty in T_P of 6 °C. The variation of mantle temperature with depth for decompression melting at constant entropy was calculated from McKenzie and Bickle's [29] expressions, and was used as the initial temperature of the mantle part of the plate. The initial crustal temperature was obtained by linear interpolation between 0 °C and the Moho temperature. The temperatures of the top and bottom boundaries of the plate were held at their initial temperatures.

The heat flux $H(n\Delta t)$ through the upper surface of the plate at time $n\Delta t$ is easily calculated from the numerical solution

$$H(n\Delta t)=\frac{k\left(T_1^n\right)\left(T_2^n-T_1^n\right)}{\Delta z} \tag{12}$$

It is straightforward to use the analytic solution to calculate the elevation of the sea floor above the asymptotic depth to which it subsides. However, the numerical calculation starts with an initial temperature and follows its evolution as the plate ages. It is therefore easier to calculate the amount of subsidence that has occurred, instead of the elevation above the asymptotic depth. The subsidence $s(t)$ below the depth of the ridge is calculated by assuming isostatic compensation

$$s(t)=\frac{1}{(\rho_0-\rho_w)}\left\{\int_0^a \rho[T(0,z)]\mathrm{d}z-\int_0^a \rho[T(t,z)]\mathrm{d}z\right\} \tag{13}$$

where $\rho_w=1.03$ Mg/m^3 the density of sea water. This expression is only accurate to $O(\alpha T)$.

2.2. Continents

The steady state temperature within old continental lithosphere was calculated by solving the relevant equations in each of the three layers shown in Fig. 4, and requiring the temperature and the heat flux to be continuous at all depths. The crust was divided into upper and lower parts, both with the same constant conductivity, 2.5 W K^{-1} m^{-1}. The value of the heat generation rate H for the upper crust was 1.12 μW m^{-3} and for the lower crust was 0.4 μW m^{-3}, the value Jaupart et al. [19] suggest for granulite. The thicknesses t_u and t_l of the upper and lower crust were varied to fit the pressure and temperature estimates from the nodules, while keeping the total crustal thickness constant. The heat generation within the thermal and mechanical boundary layers was taken to be zero, and therefore the steady state heat flux

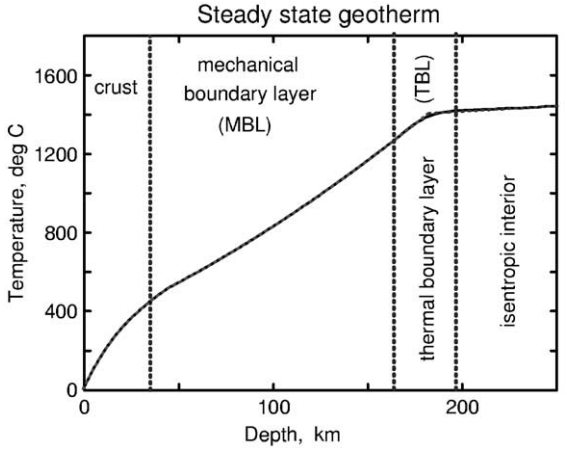

Fig. 4. The steady state thermal structure of the old lithosphere. The corresponding structure for the plate model is shown as a dotted line, only just visible in the middle of the thermal boundary layer.

throughout these layers is constant and is the same as that through the Moho, F_{moho}. If the crustal structure and heat generation, and the mantle potential temperature T_{P}, are fixed, the geotherm depends on a single parameter. This parameter was chosen to be the depth to the base of the mechanical boundary layer, z_0. The other parameters, such as the Moho heat flux, and the temperature and thickness of the thermal boundary layer, were then calculated as functions of z_0. This calculation was carried out by choosing an initial value of F_{moho} and integrating

$$k\frac{\mathrm{d}^2T}{\mathrm{d}z^2} = -H \tag{14}$$

with $T=0$ at the surface. In the crust this equation is easily solved analytically, with the crustal thickness fixed to the value obtained from seismic studies, either refraction experiments or receiver functions, and gives the Moho temperature T_{moho}. In the mechanical boundary layer (MBL) H was taken to be zero and the thermal conductivity was calculated from Eq. (4). Therefore the temperature satisfies

$$k(T)\frac{\mathrm{d}T}{\mathrm{d}z} = F_{\mathrm{moho}}. \tag{15}$$

This equation was integrated downwards using a fourth order Runge–Kutta scheme, starting at the Moho at temperature T_{moho}, to give the temperature at the base of the MBL.

The temperature within the thermal boundary layer (TBL) was determined using the same value of heat flux F_{moho} and the expressions given by Richter and McKenzie [30]. When the heat flux F_{moho} is given, the expression for the Rayleigh number Ra is

$$Ra = \frac{g\alpha d^4 F_{\mathrm{moho}}}{k\kappa\nu} \tag{16}$$

where g is the acceleration due to gravity, d the depth of the convecting layer, κ the thermal diffusivity, and ν the viscosity of the fluid. The temperature difference ΔT between the interior temperature T_{int}, obtained from $T_{\mathrm{P}}=1315$ °C, and that of the top of the TBL is then given by

$$\Delta T = 1.84\left(\frac{F_{\mathrm{moho}}d}{k}\right)Ra^{-0.219} \tag{17}$$

Clearly the temperature at the base of the MBL must be the same as that at the top of the TBL. This condition is only satisfied by one value of F_{moho}, which was found by iteration. The value of z_0 was then varied to minimise the rms misfit to the depth and temperature estimates from the nodules.

The principal reason for including the thermal boundary layer in the calculation of the steady state geotherm is for self-consistency. At the base of this layer heat transport is almost entirely by advection, whereas at the top it is entirely by conduction. In the interior of the layer the advective and conductive contributions vary smoothly to maintain a constant heat flux. In contrast, the lower boundary condition of the plate model used for the oceanic lithosphere is not self-consistent. At the base of the plate the vertical velocity is zero, and therefore the advective heat flux is also zero. However the isentropic temperature gradient, and therefore the heat flux, below the plate is not the same as that within the plate. Eq. (17) applies only when the convective circulation has reached steady state, and therefore cannot be used to calculate the temperature drop across the TBL beneath a cooling plate. Fortunately, as Fig. 4 shows, the difference between the geotherms calculated with and without the TBL is small, and indeed is scarcely visible in the plot. Therefore neglecting the existence of the TBL has a smaller effect on the variation of depth with age than does the uncertainty in $k=k(T)$.

3. Geotherms

3.1. Oceans

The subsidence of the sea floor and oceanic heat flux obtained from the numerical calculations using $k=k_{\mathrm{H}}$ in Section 2 are shown in Figs. 5 and 6, together with the observations and the curves for the analytical expressions using Parsons and Sclater's values of the constants. The numerical solution that best matches Parsons and Sclater's [13] analytical solution has $T_{\mathrm{P}}=1315$ °C, $a=106$ km and a ridge depth of 2.5 km. This potential temperature generates a crustal thickness of 7.0 km, and the rms difference between the numerical and analytical models is 53 m. The observed depths in Fig. 5 are those given by Parsons and Sclater [13] for the North Pacific. If the expression for k_{X} is used instead to calculate the

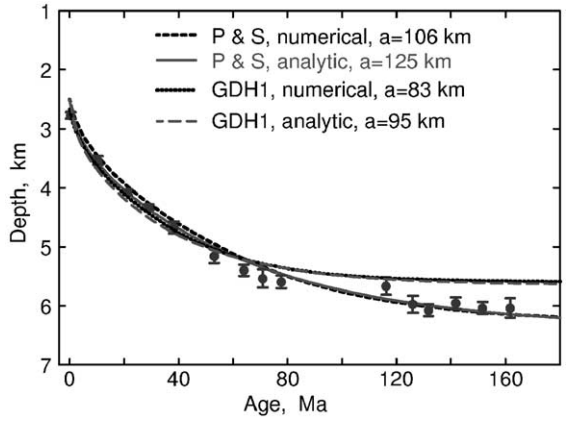

Fig. 5. The depth of the North Pacific plotted as a function of the age of the plate. The observed values and their uncertainties are from Parsons and Sclater [13]. The four curves show the analytical solution and numerical solution which best fit the analytical curve from Parsons and Sclater, labelled P&S analytic and numerical, and corresponding curves for Stein and Stein's [15] model GDH1. Both numerical solutions used $k=k_H$.

thermal evolution, the best fit has $a=110$ km, with a misfit of 54 m, and the evolution of the heat flow is indistinguishable from that of the analytic solution in Fig. 6.

Stein and Stein [15] used a temperature at the base of the lithosphere at 95 km of 1450 °C, corresponding to a potential temperature of 1408 °C. The curves in Figs. 5 and 6 were generated with this potential temperature, which produces a crustal thickness of 16 km by decompression melting. They used a ridge depth of 2.6 km, whereas 2.7 km and a plate thickness of 83 km were used for the numerical solution. The rms difference between their curve and the numerical curve is 29 m. The corresponding results for heat flow are shown in Fig. 6.The agreement between the observations and the numerical solutions in Figs. 5 and 6 is a severe test of the plate model because the only adjustable parameter is the plate thickness. The higher potential temperature of Stein and Stein's model GDH1 is not compatible with the observed crustal thickness, and is not a satisfactory model for this reason. We therefore use the numerical solution with $T_P=1315$ °C, $a=106$ km, and contours of the temperature as a function of depth and age within the lithosphere are plotted in Fig. 7a. Fig 7a and b show that the principal effect of the temperature dependence of the conductivity is to reduce the temperatures in the middle of the plate. The variation of α and k with temperature and the variable initial temperature affect the subsidence behaviour in different ways. The decrease in k with increasing T causes the temperature in the centre of the plate to be less than that of the analytic solution. Combining the increase in α with increasing temperature, this difference leads to a greater amount of subsidence. This effect is counteracted by a reduction of plate thickness, from 125 to 106 km. If α and k were constant, the variable initial temperature in Fig. 7a, which is lower than that used by Parsons and Sclater at shallow depths, would reduce the total amount of subsidence and also the gradient of the curves in Fig. 5 at ages of less than 20 Ma.

There is an important difference between models with $k=$constant and those in which it is a function of T. In the former any changes to the model parameters that affect the calculated depth-age curve also change the variation of heat flow with age. The same is not true when $k=k(T)$. Fig. 7a shows that the main effect of the temperature dependence of k is to cause the spacing between isotherms within old lithosphere to decrease with increasing depth, as the conductivity decreases with increasing temperature. The analytic solution uses a Fourier expansion of the temperature variation. Only odd terms in this expansion contribute to the depth variation, whereas both odd and even terms contribute to the heat flow. Since the principal

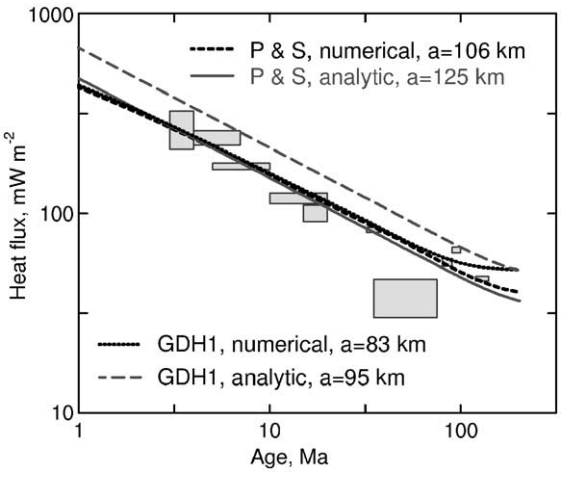

Fig. 6. Observations of the oceanic heat flow plotted as a function of age, from Sclater et al. [14]. The curves correspond to the models in Fig. 5.

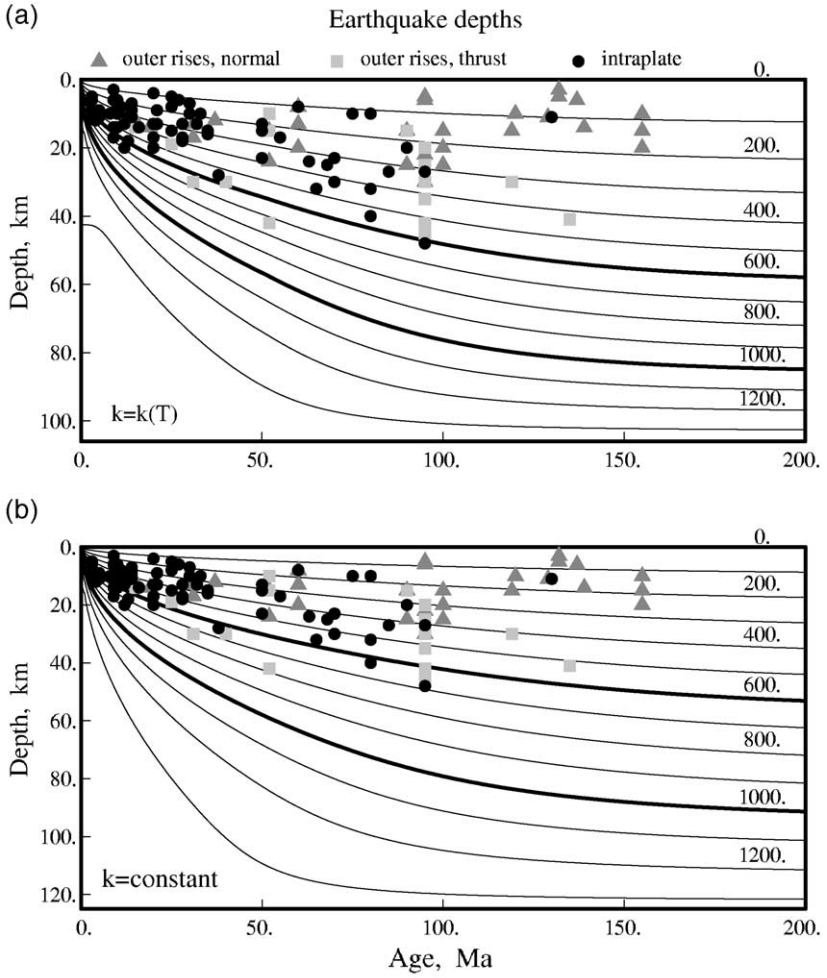

Fig. 7. The points show the depths of intraplate earthquakes within the oceanic lithosphere whose depths have been constrained by waveform modelling. (a) shows the temperature contours calculated from the numerical solution that best fits Parsons and Sclater's analytic solution, using $k=k_H$, and (b) those from the analytic solution of Parsons and Sclater [13]. The 600 and 1000 °C isotherms are marked by thick lines.

effect of $k=k(T)$ is to change the value of the first even coefficient in this expansion, different expressions for $k(T)$ can produce the same depth–age curves but different heat flow–age variation. Figs. 5 and 6 illustrate this behavior, since the two models that best fit the depth–age curves using k_H and k_X generate steady state heat flows that differ by about 3 mW m^{-2}. This behaviour may partly explain why Nagihara et al. [31] were unable to fit the depth and heat flow through the old parts of the Pacific and Atlantic Oceans with the analytic model. They found that the heat flow they calculated from the depth was on average 9.2 mW m^{-2} less than that observed. If the numerical model is used instead, this difference decreases to 6.0 mW m^{-2}. However, as Nagihara et al. point out, no cooling plate model can account for their observations in detail, because the observed heat flow is not a monotonically decreasing function of age.

Our principal concern is with the temperature at the base of the seismogenic layer. Fig. 7a shows that almost all the earthquakes occur in regions of the oceanic plate that are cooler than 600 °C. The two events that occur in hotter material are both thrusts associated with the outer rises of trenches, where the strain rates are greater than those in most interior

regions of plates. Fig. 7b shows a similar plot for Parsons and Sclater's [13] analytic model of the North Pacific, and has temperatures that are about 100 °C hotter than those in Fig. 7a in the centre of the plate.

3.2. Continents

The heat flow through the Canadian Shield has been more thoroughly investigated than has that through any other craton. The nodules from the Jericho Kimberlite in the Slave Province show a greater range of pressure and temperature than do those from any other pipe that has yet been modelled. Two sets of estimates of P and T, taken from Kopylova et al. [32], are plotted in Fig. 8, together with the best fitting geotherms calculated using the methods outlined in Section 2 using $k=k(T)$. The principal difference between the two sets of P, T estimates is the scatter about the best fitting geotherms.

Two features of these plots are particularly important. The first is that the straight line that best fits the P, T estimates does not pass through the origin in either case. This offset is the result of crustal radioactive heat generation. The heat fluxes at the surface, calculated from the geotherms, are about 52 mW m^{-2}, and those at the Moho about 13 mW m^{-2}. The surface heat flux is in good agreement with Lewis and Wang's [33] measurements of 53.3–54.4 mW m^{-2} from the southwest part of the Slave Craton; and the heat flux through the Moho is consistent with Mareschal and Jaupart's [20] estimate of 11-15 mW m^{-2} from more than a hundred measurements from the Canadian Shield. The second is the increase in temperature gradient with depth, determined from the P, T estimates from the nodules. This feature is clearer in Fig. 8a than it is in Fig. 8b, and is a common feature of P, T estimates from kimberlites (see [34]). It is commonly attributed to time-dependent heating, either by advection or shearing, associated with kimberlite emplacement. However, as Fig. 8 shows, all steady state conductive geotherms must possess this feature if the thermal conductivity decreases with increasing temperature, and therefore depth, because $k(\partial T/\partial z)$ must be the same at all depths in steady state.

Our particular concern is with the Moho temperature, which is about 500 °C in Fig. 8, and with the depth of the 600 °C isotherm, which is about 66 km. Mareschal and Jaupart [20] show that the crustal

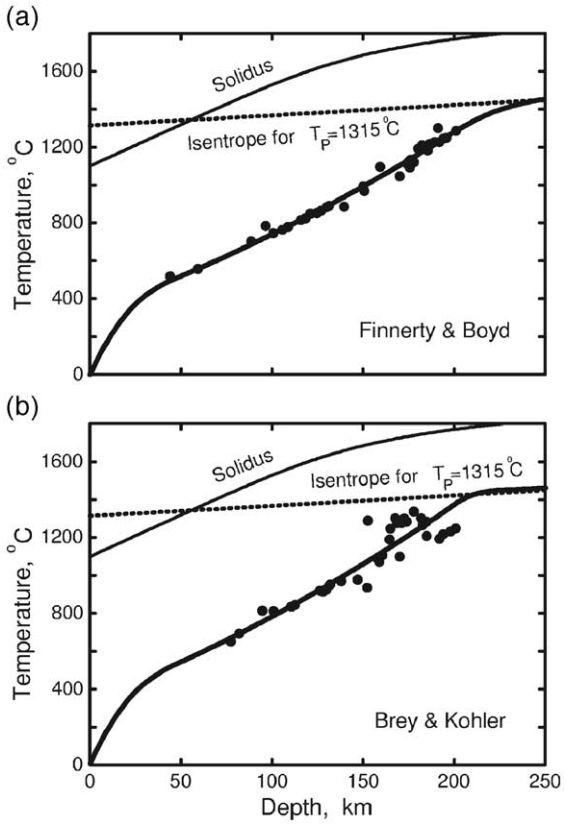

Fig. 8. Geotherms that best fit two sets of pressure and temperature estimates from the nodules from the Jericho kimberlite [32] in northern Canada. The total crustal thickness of 43 km was obtained from receiver functions (Priestly, unpublished), and that of the upper crust was taken to be 30 km. (a) Uses the expressions of Finnerty and Boyd [34] and Macgregor [38] to estimate P and T, has an rms misfit of the calculated geotherm which is 26 °C, a surface heat flux of 51.2 mW m^{-2}, a Moho heat flux of 12.4 mW m^{-2}, a Moho temperature of 491 °C and a lithospheric thickness of 226 km. (b) Uses Brey and Kohler's [39] expressions to estimate P and T, has an rms misfit of 79 °C, a surface heat flux of 52.1 mW m^{-2}, a Moho heat flux of 13.3 mW m^{-2}, a Moho temperature of 506 °C, and a lithospheric thickness of 209 km.

temperature structure of the Canadian Shield varies widely, because of variations in crustal radioactivity, even though there is little evidence for variations in the Moho heat flux. Most of the deep crustal earthquakes that Foster and Jackson [35] studied occurred in the mobile belts surrounding Archaean cratons, rather than in their interiors. A detailed study of the crustal thickness in southern Africa by Nguuri et al. [36] using receiver functions showed that the crustal thickness in the mobile belts was 45–50 km, and was

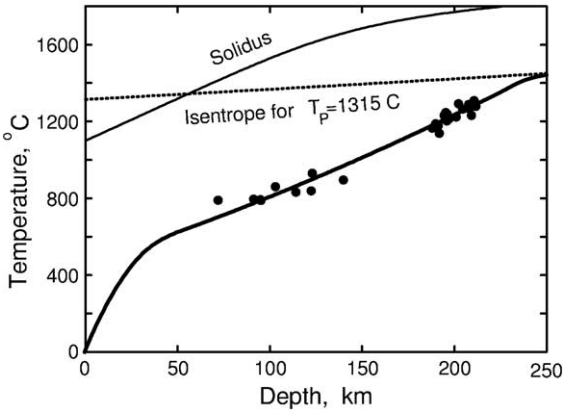

Fig. 9. Geotherm that best fits the pressure and temperature estimates from the Udachnaya kimberlite in central Siberia [40]. The surface heat flux is 58.6 mW m^{-2}. The crustal thickness is assumed to be 50 km, and that of the upper crust to be 40 km. The Moho temperature is 627 °C, and the lithospheric thickness is 242 km.

systematically thicker than that beneath the interiors of the cratons. Durrheim and Mooney [37] showed that the thickness of the Proterozoic crust, of which most mobile belts consist, is about 40–50 km.

Fig. 9 shows a geotherm that fits the nodules from the Udachnaya Kimberlite, on the Siberian Shield. The temperature gradient in the mantle is less than that in Fig. 8, and therefore the crustal heat generation rate and Moho temperature must be greater. The best fitting geotherm has a Moho heat flux of about 10 mW m^{-2} and a Moho temperature greater than 600 °C. Geotherms of mobile belts are likely to resemble that in Fig. 9 more than those in Fig. 8, because of their crustal thickness, and therefore to have Moho temperatures of 600 °C or more.

4. Discussion

The most important result of this study of the temperatures within oceanic and continental plates is that there is no convincing evidence that the rheology of continental and oceanic mantle is different. Most earthquakes occur in crustal or mantle material that is cooler than 600 °C. The few exceptions occur in oceanic mantle where the strain rates are particularly large. Probably the temperature dependence of the thermal conductivity is now the least well known parameter that affects the calculated oceanic geotherms, and results in an uncertainty in lithospheric temperature of about 50 °C. Beneath shields, the principal controls on the Moho temperature are the crustal thickness and crustal radioactivity. As Nguuri et al. [36] show, the crustal thickness can now be easily obtained from receiver functions. The crustal radioactivity is harder to estimate, and requires the type of study that has been carried out by Mareschal and Jaupart. The uncertainty in the Moho temperature of shields is therefore probably about 100 °C. It is therefore still possible that the rheologies of oceanic and continental mantle are affected by composition as well as temperature. However, we have found no evidence that compositional effects are required by the existing observations.

The difference between the Moho temperatures at Jericho and Udachnaya suggest that there may be regions where continental seismicity extends from the crust into the mantle beneath the Moho. Such behaviour is most likely to occur where the crust is thin and earthquakes occur in Archaean cratons. Teleseismic waveform modelling requires events whose magnitude is about 5.5 or greater. Though no such events have yet been found (Fig. 1), the arguments above suggest that they may occur, though they are likely to be rare.

Another important result of this study is that the plate model still fits the observations of depth and heat flow in the oceans excellently, even when k, C_P and α are constrained by laboratory measurements and are taken to be temperature dependent, the potential temperature at the base of the plate is constrained to be 1315 °C, and the initial temperature of the plate is that resulting from isentropic decompression. Though the only adjustable parameter is then the plate thickness, the fits to the variation of heat flow and depth with age are at least as good as those of the analytic model with constant and adjustable coefficients. The principal difference between the numerical model with variable coefficients and the standard analytic model is that the temperature in the central part of old oceanic plates is about 100 °C less than that of the standard model.

Steady state conductive geotherms for old continental regions are also in excellent agreement with heat flow measurements and with P, T estimates from kimberlite nodules. Here the main difference from older models is that the crustal contribution to the heat

flow is increased, and the mantle heat flow is decreased. The decrease in $k(T)$ with increasing temperature causes the temperature gradient in the mantle part of the lithosphere to increase with depth. The increase in the crustal contribution to the heat flow and crustal thicknesses of 45–50 km produce Moho temperatures of 600 °C or more in the mobile belts surrounding cratons where most earthquakes occur.

5. Conclusions

By far the most important result of this study is that almost all mantle earthquakes occur in material whose temperature is less than 600 °C. This result accounts for the absence of earthquakes below the Moho in shields, and their depth distribution in oceanic lithosphere. The only exceptions occur in regions where the strain rate is high, on the outer rises of trenches. The simple analytic model of a cooling oceanic plate requires the thermal conductivity to be constant. In fact the thermal conductivity decreases with increasing temperature, and this effect causes the central temperature of the plate to be about 100 °C less than that of the analytic model. Beneath shields the Moho temperature is controlled principally by the crustal thickness and crustal heat generation rate, both of which have larger values than has generally been assumed, leading to higher Moho temperatures.

Acknowledgements

We would like to thank P. Asimow, J. Hillier, C. Jaupart, D. Sandwell and J. Sclater for their help, and the Royal Society for support.

References

[1] A.B. Watts, Isostasy and Flexure of the Lithosphere, Cambridge University Press, 2001.
[2] R. White, D. McKenzie, R.K. O'Nions, Oceanic crustal thickness from seismic measurements and rare earth element inversions, J. Geophys. Res. 97 (1992) 19683–19715.
[3] D.A. Wiens, S. Stein, Age dependence of intraplate seismicity and implications for lithospheric evolution, J. Geophys. Res. 88 (1983) 6455–6468.
[4] W.P. Chen, P. Molnar, Focal depths of intracontinental and intraplate earthquakes and their implications for the thermal and mechanical properties of the lithosphere, J. Geophys. Res. 88 (1983) 4183–4214.
[5] A. Maggi, J.A. Jackson, K. Priestley, C. Baker, A reassessment of focal depth distribution in southern Iran, the Tien Shan and northern India: do earthquakes really occur in the continental mantle?, Geophys. J. Int. 143 (2000) 629–661.
[6] S. Mitra, K. Priestley, A.K. Bhattacharyya, V.K. Gaur, Crustal structure and earthquake focal depths beneath northeastern India and southern Tibet, Geophys. J. Int. 159 (2005) 227–248.
[7] J.A. Jackson, H. Austrheim, D. McKenzie, K. Priestley, Metastability, mechanical strength, and support of mountain belts, Geology 32 (2004) 625–628.
[8] D.W. Forsyth, Subsurface loading and estimates of the flexural rigidity of continental lithosphere, J. Geophys. Res. 90 (1985) 12623–12632.
[9] D. McKenzie, D. Fairhead, Estimates of the effective elastic thickness of continental lithosphere from Bouguer and free air gravity anomalies, J. Geophys. Res. 102 (1997) 27523–27552.
[10] D. McKenzie, Estimating T_e in the presence of internal loads, J. Geophys. Res. 108 (B9) (2003) 2438, doi:10.1029/2002JB001766. 21 pp.
[11] A. Maggi, J.A. Jackson, D. McKenzie, K. Priestley, Earthquake focal depths, effective elastic thickness, and the strength of the continental lithosphere, Geology 28 (2000) 459–498.
[12] I.M. Artemieva, W.D. Mooney, Thermal thickness and evolution of Precambrian lithosphere: a global study, J. Geophys. Res. 106 (2001) 16387–16414.
[13] B. Parsons, J.G. Sclater, An analysis of the variation of ocean floor bathymetry and heat flow with age, J. Geophys. Res. 82 (1977) 803–827.
[14] J.G. Sclater, C. Jaupart, D. Galson, The heat flow through oceanic and continental crust and the heat loss of the earth, Rev. Geophys. Space Phys. 18 (1980) 269–311.
[15] C.A. Stein, S. Stein, A model for the global variation in oceanic depth and heat flow with lithospheric age, Nature 359 (1992) 123–130.
[16] M.P. Doin, L. Fleitout, Thermal evolution of the oceanic lithosphere: an alternative view, Earth Planet. Sci. Lett. 142 (1996) 121–136.
[17] H.N. Pollack, D.S. Chapman, On the regional variation of heat flow, geotherms, and lithospheric thickness, Tectonophysics 38 (1977) 279–296.
[18] C. Jaupart, J.C. Mareschal, The thermal structure and thickness of continental roots, Lithos 48 (1999) 93–114.
[19] C. Jaupart, J.C. Mareschal, L. Guillou-Frottier, A. Davaille, Heat flow and thickness of the lithosphere in the Canadian Shield, J. Geophys. Res. 103 (1998) 15269–15286.
[20] J.C. Mareschal, C. Jaupart, Variations of surface heat flow and lithospheric thermal structure beneath the North American craton, Earth Planet. Sci. Lett. 223 (2004) 65–77.
[21] D. McKenzie, Some remarks on heat flow and gravity anomalies, J. Geophys. Res. 72 (1967) 6261–6273.
[22] J.F. Schatz, G. Simmons, Thermal conductivity of Earth materials at high temperature, J. Geophys. Res. 77 (1972) 6966–6983.

[23] Y. Xu, T.J. Shankland, S. Linhardt, D.C. Rubie, F. Lagenhorst, K. Klasinsk, Thermal diffusivity and conductivity of olivine, wadsleyite and ringwoodite to 20 GPa and 1373 K, Phys. Earth Planet. Inter. 143–144 (2004) 321–336.
[24] A. Hofmeister, Mantle values of thermal conductivity geotherm from phonon lifetimes, Science 283 (1999) 1699–1709.
[25] M.A. Bouhifid, D. Ardrault, G. Fiquet, P. Richet, Thermal expansion of forsterite up to the melting point, Geophys. Res. Lett. 10 (1996) 1143–1146.
[26] R.G. Berman, L.Y. Aranovich, Optimized standard state and solution properties of minerals: 1. Model calibration for olivine, orthopyroxene, cordierite, garnet, and ilmenite in the system FeO–MgO–CaO–Al_2O_3–TiO_2–SiO_2, Contrib. Mineral. Petrol. 126 (1996) l–24.
[27] W.H. Press, S.A. Teukolsky, W.T. Vetterling, B.P. Flannery, Numerical Recipes, Cambridge University Press, 1992.
[28] H. Kogitani, M. Akogi, Melting enthalpies of mantle peridotite: calorimetric determinations in the system CaO–MgO–Al_2O_3–SiO_2 and application to magma generation, Earth Planet. Sci. Lett. 153 (1997) 209–222.
[29] D. McKenzie, M.J. Bickle, The volume and composition of melt generated by extension of the lithosphere, J. Petrol. 29 (1988) 625–679.
[30] F.M. Richter, D. McKenzie, Parameterizations for the horizontally averaged temperature of infinite Prandtl number convection, J. Geophys. Res. 86 (1981) 1738–1744.
[31] S. Nagihara, C.R.B. Lister, J.G. Sclater, Reheating of old oceanic lithosphere: deductions from observations, Earth Planet. Sci. Lett. 139 (1996) 91–104.
[32] M.G. Kopylova, J.K. Russell, H. Cookenboo, Petrology of peridotite and pyroxenite xenoliths from the Jericho kimberlite: implications for thermal state of the mantle beneath the Slave craton northern Canada, J. Petrol. 40 (1998) 79–104.
[33] T.J. Lewis, K. Wang, Influence of terrain on bedrock temperatures, Global Planet. Change 98 (1992) 87–100.
[34] A.A. Finnerty, F.R. Boyd, Thermobarometry for garnet peridotites: and compositional structure of the upper mantle, in: P.H. Nixon (Ed.), Mantle Xenoliths, J. Wiley & Sons, New York, 1987, pp. 381–402.
[35] A.N. Foster, J.A. Jackson, Source parameters of large African earthquakes: implications for crustal rheology and regional kinematics, Geophys. J. Int. 134 (1998) 422–448.
[36] T.K. Nguuri, J. Gore, D.E. James, S.J. Webb, C. Eright, T.G. Zengeni, O. Gwavava, J.A. Snoke, Kaapvaal Seismic Group, Crustal structure beneath southern Africa and its implications for the formation and evolution of the Kaapvaal and Zimbabwe cratons, Geophys. Res. Lett. 28 (2001) 2501–2504.
[37] R.J. Durrheim, W.D. Mooney, Evolution of the Precambrian lithosphere: seismological and geochemical constraints, J. Geophys. Res. 99 (1994) 15359–15374.
[38] I.D. Macgregor, The system MgO–Al_2O_3–SiO_2: solubility of $A1_2O_3$ in enstatite for spine1 and garnet peridotite compositions, Am. Mineral. 59 (1974) 110–119.
[39] G.P. Brey, T. Kohler, Geothermobarometry in four-phase lherzolites: II. New thermobarometers, and practical assessment of existing thermobarometers, J. Petrol. 31 (1990) 1353–1378.
[40] F.R. Boyd, N.P. Pokhilenko, D.G. Pearson, S.A. Mertzman, N.V. Sobolev, L.W. Finger, Composition of the Siberian cratonic mantle: evidence from Udachnaya peridotite xenoliths, Contrib. Mineral Petrol. 128 (1997) 228–246.